



# A study on film hole drilling of IN718 superalloy via laser machining combined with high temperature chemical etching

Qiang Zhang<sup>1,2</sup> · Shu-Feng Sun<sup>1,2</sup> · Feng-Yun Zhang<sup>1,2</sup> · Jin Wang<sup>1,2</sup> · Qiang-Qiang Lv<sup>1,2</sup> · Yong Shao<sup>1,2</sup> · Qing-Yu Liu<sup>1,2</sup> · Jing Shao<sup>1,2</sup> · Xin-Fu Liu<sup>1,2</sup> · Yan Zhang<sup>1,2</sup>

Received: 18 June 2019 / Accepted: 1 October 2019 / Published online: 20 November 2019  
© Springer-Verlag London Ltd., part of Springer Nature 2019

## Abstract

A novel method of laser machining combined with high temperature chemical etching (LMHTCE) was proposed. This novel method can take full advantage of both approaches to drill film holes in an IN718 superalloy without a recast layer or a heat affect zone (HAZ). A solution of hydrochloric acid and sodium nitrate, which minimally reacts with IN718 at room temperature but rapidly reacts under high temperatures, was tested and chosen. Holes drilled in air, water, and chemical solutions by a pulsed laser of 1064 nm were studied, and scanning electron microscope (SEM) and energy dispersive spectrometer (EDS) were employed to detect the morphology of the holes and the elemental distribution in different zones. The holes processed in the chemical solution had fewer defects compared with those in the other two mediums. The defocusing distance parameter was optimized to minimize the hole diameter and taper. When the defocusing distance was 0  $\mu\text{m}$  in the drilling stage and  $-60 \mu\text{m}$  in the high temperature chemical etching stage, a hole with a smaller diameter and taper can be obtained.

**Keywords** Laser machining · High temperature chemical etching · IN718 · Film holes

## 1 Introduction

The material of turbine blades requires specific properties, such as a high creep and fatigue strength, good oxidation and hot corrosion resistance, and long-term structural stability, to withstand the strains of the working environment. Ni-based superalloys are often chosen due to their superior chemical and mechanical properties [1]. Meanwhile, film cooling holes are introduced to extend the working life of turbine components because they can produce a cooling film between the hot flow and the turbine blades [2].

The diameters of film cooling holes vary in the range of 0.25–1.0 mm, and manufacturing such holes in Ni-based superalloys is difficult. Various methods of manufacturing film

holes, such as mechanical drilling [3], electrical discharge drilling [4], laser drilling [5], electrochemical drilling [6], and additive manufacturing [7], have been studied. Laser drilling is an ideal way to produce holes with better quality and is the most effective technique compared with the other methods. However, drilling with a laser has serious defects, such as heat affect zone (HAZ), recast layers, and microcracks, which can significantly influence the cooling effectiveness and fatigue life of a turbine blade [8]. Thus to achieve a high efficiency and a thinner defect layer, parameters, such as peak power, average power, pulse duration, and focal position, have been researched to optimize the laser drilling processes [9–13]. The modeling, simulation, and analysis of the film hole and laser processing have also been studied [14–17]. In previous studies, the recast layer and HAZ have been minimized, but they cannot be removed completely.

The liquid-assisted laser ablation process is a combined machining technique, which can cut and cool a workpiece and simultaneously decrease the HAZ thickness in the laser ablation material processing [18]. The mechanism in the processing is very complicated for drilling in liquid; incident laser pulses are stretched or compressed, self-focused, and scattered on surface waves and bubbles [19]. The formation of a deep superheated liquid with bubbles and subsequent melt

✉ Shu-Feng Sun  
shufeng2001@163.com

<sup>1</sup> Collaborative Innovation Center for Green Intelligent Laser Manufacturing Technology and Equipment of Shandong Province, Qingdao 266520, China

<sup>2</sup> Shandong Research Center of Laser Green and High Efficiency Intelligent Manufacturing Engineering Technology, Qingdao University of Technology, Qingdao 266520, China

expulsion is a dominant mechanism for nanosecond pulsed laser ablation [20, 21]. These phenomena could lead to a hole-like surface or a porous thin film on the sample surface [22, 23]. In addition, drilling IN718 samples in water can yield larger holes with less debris and spatter compared with air drilling [24], but the inside surface of these holes is rougher. Li and Achara [25] found that a groove can be milled on stainless steel in a salt solution by a laser with no heat affect zone or recast present. The application of the laser beam can significantly accelerate the chemical reaction. Li et al. [26] used the electrolytes which contained  $\text{NaNO}_3$  in laser-electrolytic machining to improve the quality of the inner hole. Stephen [27] machined high precision grooves in nitinol using a similar process, but the machining efficiency of the low-power laser machining was lower. Zhang et al. [28] proposed an in situ combined tubular electrode electro-discharge high-speed drilling electrochemical machining process to improve the quality of holes and to remove the recast layer. Khuat et al. [29] fabricated holes in SiC and immersed them in a chemically selective etching solution to remove the laser-affected zones. Therefore, the combination of chemicals can be a good method to remove defects.

In this study, laser machining combined with high temperature chemical etching (LMHTCE) was proposed to machine holes in IN718 to get a hole with high quality. A special chemical solution, which could react violently with IN718 under high temperatures but will not react at room temperature, was chosen. The detailed morphology of the holes drilled in air, water, and chemical solutions were studied. The effects of the defocusing distance on the hole diameter and taper were analyzed.

## 2 Experimental details

### 2.1 Material and equipment

IN718 is used in this study. The size of the samples was  $20 \times 20 \times 1.5 \text{ mm}^3$ , and the chemical composition is shown in Table 1. An electronic balance (Sartorius, BSA224S) with a maximum weight of 220 g, a precision of 1/10000 g, and a deviation of 0.1 mg was used to measure the weight of the samples. An electronic hot plate ANSAI946C+, with a range of controlled temperatures of approximately  $0 \text{ }^\circ\text{C}$ – $400 \text{ }^\circ\text{C}$  and a controlling accuracy of  $\pm 1 \text{ }^\circ\text{C}$ , was used to maintain a constant temperature in the study. Distilled water was used to dilute the chemical solution. Samples are mounted, ground, polished, and dipped in a metallographic etchant to analyze

the oxide layer, the recast layer, and the HAZ along the mid-cross section of the holes.

SEM (HITACHI S-3400 N) was employed to observe the morphology of the holes and to measure the thickness of the recast and oxide layers. An EDS was applied to analyze the element types and contents in a micro-area of the material. An IPG ytterbium pulsed fiber laser, capable of operating at a maximum average power of 200 W with a pulse repetition rate from 200 to 2000 kHz and an optical quality of  $M^2 = 1.3$ , was used in this investigation. A lens with a focal length of 254 mm is used to focus the beam onto the surface of the work piece, and the focal spot diameter and maximum laser beam intensity were calculated to be 0.067 mm and  $5.6 \text{ kW/mm}^2$ , respectively.

The formulas for the hole taper and the single pulse energy are as follows:

$$C = (D-d)/L \quad (1)$$

$$E = P/F \quad (2)$$

where  $C$  is the taper of the hole,  $D$  is the diameter of the entrance hole,  $d$  is the diameter of the exit hole,  $L$  is the thickness of the sample,  $E$  is the single-pulse energy,  $P$  is the laser power, and  $F$  is the laser frequency.

### 2.2 Machining principles and procedures

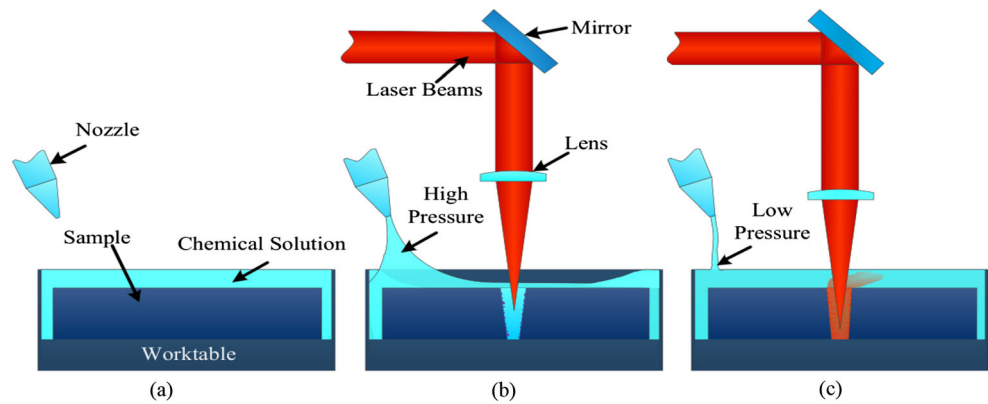
The processes of LMHTCE are illustrated in Fig. 1. In the preparation stage, the sample is fixed on the worktable and dipped in the chemical solution, as shown in Fig. 1 a. The chemical solution thickness on the sample was 4 mm. During the drilling stage, the high-pressure chemical solution is ejected from the nozzle on the side axis to form a solution layer with a thickness of approximately 0.2 mm on the surface of the sample, as shown in Fig. 1 b. On the sample surface, a very thin layer of water formed by pressure can greatly reduce the absorption of the laser. In addition, the high-speed flowing solution can remove a large amount of heat and part of the debris generated by the laser processing. However, after drilling, the oxide layer, recast layer, and HAZ were still observed around the hole.

In the high temperature chemical etching stage, the laser frequency is adjusted to the maximum value, as shown Fig. 1 (c). According to eq. (2), under the same laser power, when the laser frequency increases, the energy of the laser pulse decreases, and the heating effect on the solution is approximately uniform. In addition, adjusting the laser defocusing distance can reduce the hole taper to some extent. The liquid

**Table 1** Chemical composition of parent metals in wt.%

Element	Ni	Cr	Fe	Nb	Mo	Ti	Co	Cu	Si	Mn	C
Wt.%	53.66	18.41	17.9	4.92	2.87	0.96	0.34	0.13	0.09	0.08	0.03

**Fig. 1** The schematic of the whole LMHTCE processes: **a** preparing stage, **b** drilling stage, **c** high temperature chemical etching stage



flowing out of the side axis nozzle was adjusted to the low-pressure state so that the liquid on the surface of the sample will be restored to its original state with a 4 mm liquid layer. New liquid will be added continuously to maintain the fluidity of the liquid on the surface of the sample to prevent the solution from boiling. Bubbles can reflect and deflect the laser beam, which could ablate the hole without direction instead of removing defects. The heated chemical solution that accumulates at the orifice can be diluted in time to further reduce the reaction between the hot chemical solution and the matrix at the entrance hole.

### 3 Results and discussion

#### 3.1 Selection of chemical solution

Given the strong etching resistance of nickel-based alloys, mixtures of hydrochloric acid (HCl), nitric acid (HNO<sub>3</sub>), and sulfuric acid (H<sub>2</sub>SO<sub>4</sub>) were chosen. The concentration of each acid is 1 mol/L. The samples are weighed and dipped into the solutions for 2 h at 20 °C and 90 °C. The temperature of 90 °C is chosen to prevent the solution from boiling and the water from evaporating, which would change the concentration of the acid.

The weight loss of the samples in the different chemical solutions at 20 °C and 90 °C is shown in Table 2. Only the mixture of HCl and HNO<sub>3</sub> obviously reacted with the samples at 20 °C or 90 °C compared with the other mixtures. Furthermore, different concentrations of the mixtures of HCl and HNO<sub>3</sub> were tested, and the sodium nitrate crystal was chosen instead of HNO<sub>3</sub> to avoid excessive hydrogen ions.

**Table 2** The weight loss of samples in different chemical solutions in 20 °C and 90 °C (mg)

Temperature (°C)	HCl+H <sub>2</sub> SO <sub>4</sub>	HCl +HNO <sub>3</sub>	HNO <sub>3</sub> +H <sub>2</sub> SO <sub>4</sub>
20	0.20	7.20	0.70
90	0.80	27.10	3.00

The reaction results of the sample in different concentrations of the mixture of HCl and NaNO<sub>3</sub> are shown in Fig. 2. An HCl concentration of 5 mol/L was not studied because, at this concentration, NaNO<sub>3</sub> was saturated.

Generally, NO<sub>3</sub><sup>-</sup> is a strongly oxidizing ion in the acid solution, and a dense oxide film will form on the metal surface to limit the reaction to a certain extent. Halogen group elements have an activation effect and can accelerate the reaction to a certain degree, and the chloride ion is one of the halogen group elements that can also, theoretically, promote the reaction. The results shown in Fig. 2 a are not consistent with this theory because of measurement errors, and the weight loss are small due to the weak reaction at room temperature. However, at 90 °C, the reaction rate increased as the chloride ion concentration increased, as shown in Fig. 2 b.

The reaction rate at 90 °C was greatly increased, with the weight loss increased by an order of magnitude compared with that at 20 °C, as shown in Fig. 2 a. The sample was greatly corroded when the chemical solution was in the following proportion: 1 mol/L NaNO<sub>3</sub> with 3 mol/L HCl, 1 mol/L NaNO<sub>3</sub> with 4 mol/L HCl, and 2 mol/L NaNO<sub>3</sub> with 4 mol/L HCl. However, these solutions were not chosen because they can react with the sample at 20 °C. In the remaining experiment groups, a mixture of 4 mol/L NaNO<sub>3</sub> and 3 mol/L HCl was chosen because, under this combination, the weight loss of the sample was the largest at 90 °C and almost zero at 20 °C.

#### 3.2 Comparison under three processing conditions

In the drilling stage of LMHTCE, to verify the advantages of processing in the chemical solution, experiments were also carried out under water and air media. The laser processing parameters are as follows: repeat frequency 200 kHz, power 200 W, point processing time 500 ms, repeat times 10 times.

SEM micrographs of a hole drilled (1) in air, (2) in water, and (3) in the chemical solution are shown in Fig. 3. In Fig. 3, (a) indicates a micrograph of the entry side of the hole, (b) indicates the cross sections of the hole, and (c) is a

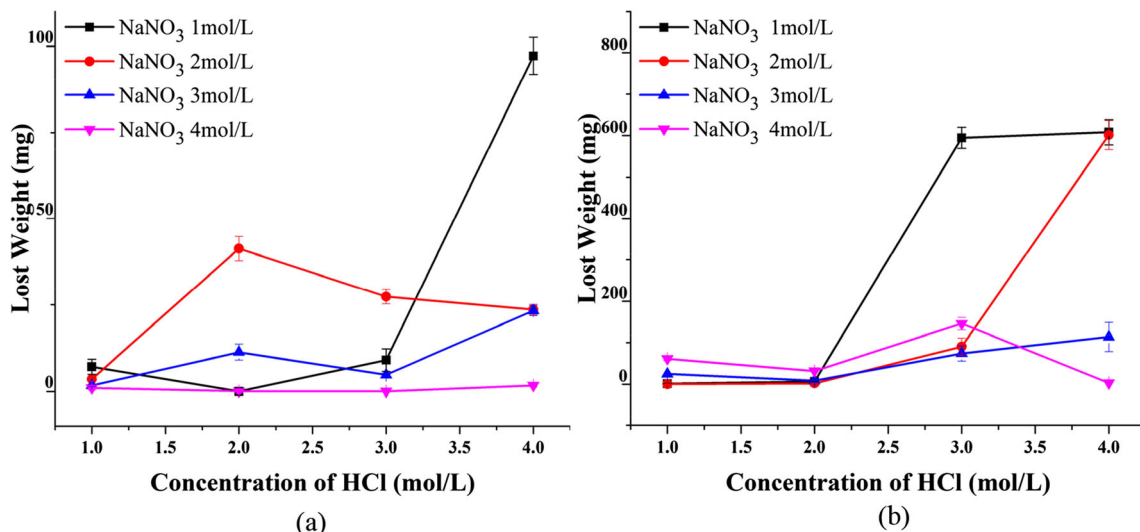


Fig. 2 The lost weight of samples in different concentrations of chemical solutions under two temperatures: a 20 °C and b 90 °C

magnification of the area marked with a rectangle in (b). Moreover, dotted lines are used to distinguish the boundaries of the recast layer, HAZ, and metal matrix.

For the samples drilled in air, the metal melted, and the hole was blocked by the melted metal, which caused the large energy of the laser, as shown in Fig. 3 (a1). In Fig. 3 (c1),

the characteristics of the three regions are obvious. The grain size of the HAZ is larger than the grain of the recast layer and the metal matrix. In addition, the etch pits in Fig. 3 (b1) are generated by the corrosion caused by the metallographic etchant. The bubble pits are formed by air trapped in the molten metal. As shown in Fig. 3 (a2), due to the large pulse energy of

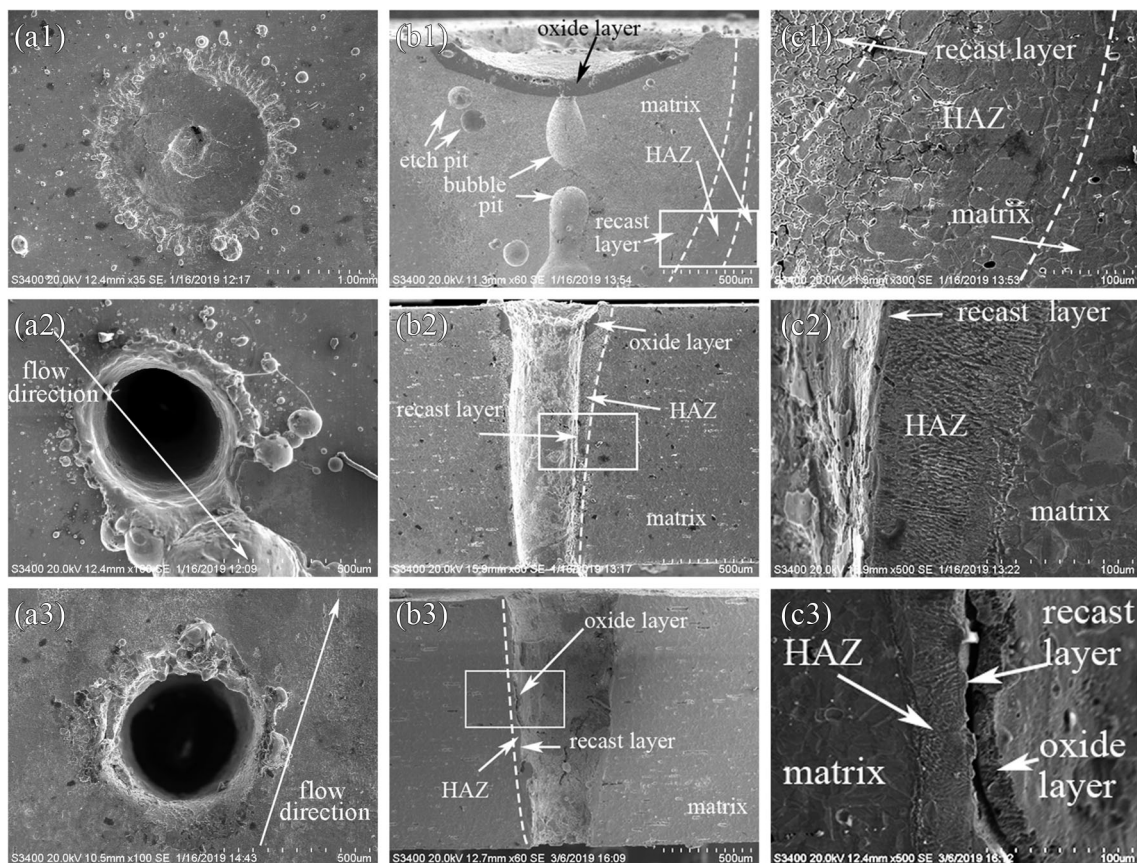


Fig. 3 The SEM micrographs of a hole drilled in different conditions: (1) in air, (2) in water, (3) in chemical solution. (a) The entry side of hole. (b) The cross section of hole. (c) The local amplification of (b)

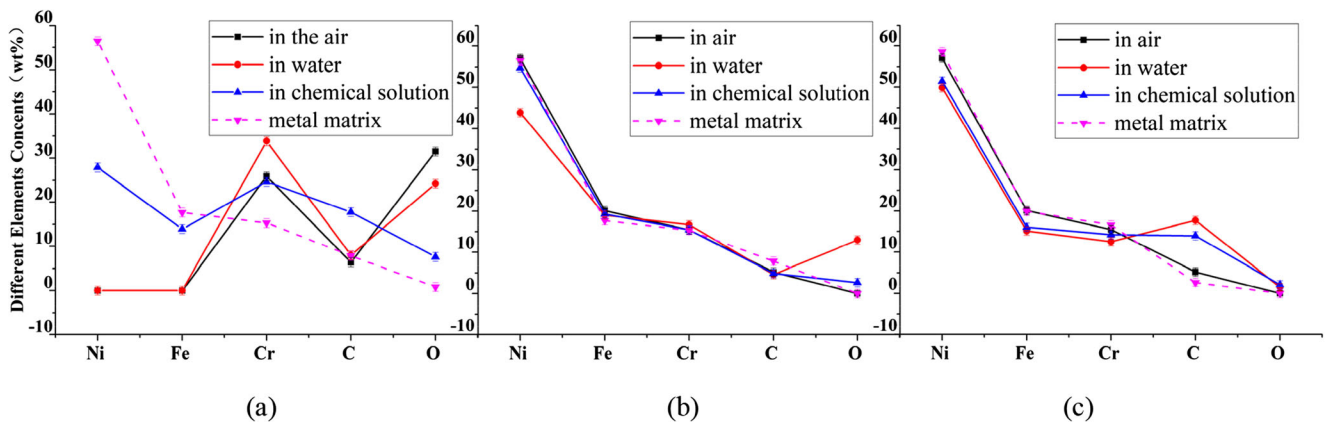


Fig. 4 Main elements contents in a oxide layer, b recast layer, and c HAZ on three process conditions

the lasers, the materials melted and exploded instantaneously, molten metal accumulated at the hole entrance, and many splashes solidified into metal balls around the hole due to the water. Furthermore, a large molten ball solidified at the bottom right corner of the orifice. The splashes concentrated on the other side of the hole. As shown by the flow direction in Fig. 3 (a2), the thickness of the molten material increases gradually along the same direction. Fig. 3 (b2) shows the cross section of the hole drilled in water. The oxide layer adhered to the upper part of the hole, and the average thickness of the HAZ is approximately 94  $\mu\text{m}$ .

Fig. 3 (a3) shows that the generated debris reacted with the chemical solution during the laser drilling; the amount of the debris is visibly declined; the matrix of the orifice remained stable, and there was no obvious sign of corrosion compared with the holes drilled in air and water, as shown in Fig. 3 (a1) and (a2). Meanwhile, as shown in Fig. 3 (a3), the distribution of the residues around the entrance of the holes drilled in the chemical solution shows a certain directivity, which accounts for the direction of the flow during drilling. In Fig. 3 (b3), most of the oxide layer was removed by the process, but a small part of the oxide layer remained on the inner surface of

the hole. The gap between the oxide layer and the recast layer is clear in Fig. 3 (c3), but the layers are tightly coupled after drilling in water, as shown in Fig. 3 (c2). Figure 3 (c3) reveals that the chemical solution can react and remove most of the defect layer. The recast layer is thinner than that in Fig. 3 (c2), and the thickness of the HAZ was effectively reduced to approximately 38  $\mu\text{m}$ . The diameter of the hole was also enlarged by approximately 110  $\mu\text{m}$  on average compared with the holes drilled in water. However, the pore size increased and was much larger than the thickness of the thinned recast layer and the HAZ, which indicates that processing by chemical reaction could increase the removal efficiency of drilling.

As Table 1 shows, nickel (Ni), iron (Fe), and chromium (Cr) are the main elements in IN718. In different processing methods, the contents of different elements in different zones varied, and the physical and chemical properties of the materials also changed at the same time. The contents of the main elements in (a) the oxide layer, (b) the recast layer, and (c) the HAZ for the three processing media are shown in Fig. 4. Figure 4 a shows the contents of the main elements in the oxygen layer drilled in the three media. For the holes drilled in air and water, the

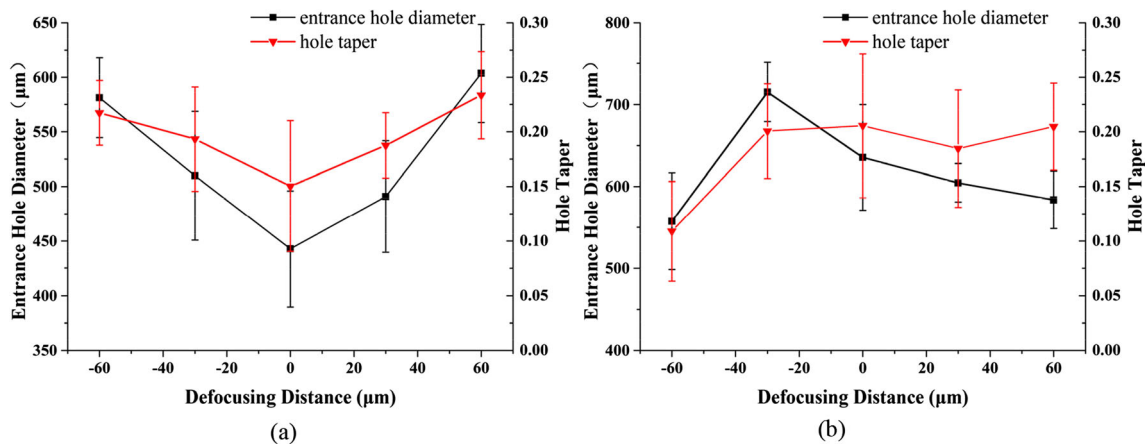
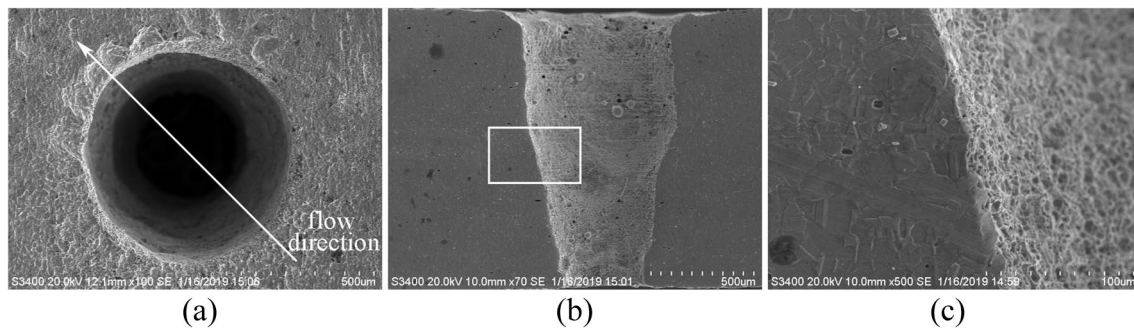


Fig. 5 The variation of entrance hole diameter and hole taper with different defocusing distance under two processing conditions: a only drilling stage b whole process of LMHTCE 1 solution



**Fig. 6** The SEM micrographs of a hole processed by LMHTCE. **a** The entry side of hole. **b** The cross section of hole. **c** The local amplification of **b**

proportion of oxygen and Cr increased, and the contents of Ni and Fe are almost zero. In the same zone, for the holes processed in the chemical solution, Ni and Fe are retained, their contents decreased, and the Ni content is halved compared with that in the metal matrix. That the contents of Ni and Fe did not decrease to zero demonstrates that the reaction of the chemical solution accelerated the removal of the material in the drilling stage of LMHTCE. Before Ni and Fe are completely removed by the laser, new Ni and Fe can be added to the oxide layer in time. In addition, carbon was accumulated at the same time. Thus, in the oxide layer, the proportion of carbon also increased after drilling in the chemical solution, as shown in Fig. 4 a.

In the oxide layer, under the three processing conditions, only the Cr content is relatively stable. This means that in the drilling stage, Ni and Fe have a higher absorptivity to the laser wavelength compared with Cr, so they are more easily removed. There is no doubt that the oxygen content increased significantly in the oxide layer compared with that in the matrix. The content of oxygen is relatively lower when the holes are processed in water and the chemical solution compared with air, indicating that processing in a solution can prevent further oxidation of the material to a certain extent.

In Fig. 4 b, the main difference of the elemental contents in the recast layer is the proportion of oxygen. The oxygen content in the recast layer for the sample drilled in water is higher

than that for the sample drilled in the chemical solution and almost zero for the sample drilled in air. The oxygen content in the oxide layer was halved in the recast layer for the samples drilled in water and the chemical solution. The contents of the other elements are similar to those in the matrix. Unlike the formation of the oxide layer, the recast layer was not directly laser processed, and its composition did not change dramatically.

For the elemental contents of the HAZ, which are shown in Fig. 4 c, the main difference is the content of carbon. For the samples processed in water and the chemical solution, the carbon content was approximately twice as large as that for the sample processed in air.

### 3.3 Laser machining combined with high temperature chemical etching

In the high temperature chemical etching stage of LMHTCE, the laser processing parameters are as follows: repeat frequency 2000 kHz, power 160 W, processing time 500 ms, and repeat time 20 times. In this section, the defocusing position was chosen to optimize the LMHTCE results.

As Fig. 5 a shows, after the drilling stage, when the defocusing distance was zero, the minimum hole taper appeared. Meanwhile, the diameter of the entrance hole was approximately 450  $\mu\text{m}$ , which was also the smallest hole. Figure 5 b illustrates the holes processed by LMHTCE with

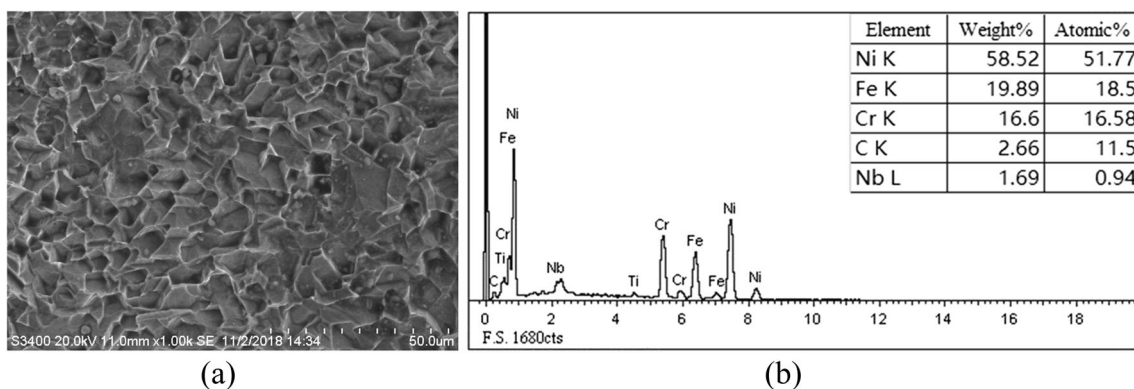


**Fig. 7** The SEM micrograph **(a)** and EDS graph **(b)** of the inner surface of the hole

various defocusing distances. In the drilling stage, the 0  $\mu\text{m}$  defocusing distance was chosen for thinner prefabricated holes with a smaller taper. In the next stage, when the defocusing distance was  $-60\ \mu\text{m}$ , the smallest hole taper and the minimum hole diameter were observed.

Figure 6 shows the SEM micrographs of a hole processed by LMHTCE. In Fig. 6 a, no oxides or other impurities are deposited at the orifice, but the orifice is still partially etched by the laser-heated chemical solution that accumulated at the orifice. The etched position is related to the flow direction of the solution. Figure 6 c reveals that the recast layer and the HAZ are completely removed.

Figure 7 shows the SEM micrograph of the inner surface of the hole drilled by LMHTCE enlarged 1000 $\times$ . The irregular honeycomb structure can be clearly seen. This structure is mainly due to the non-directionality of the chemical reactions. Moreover, in the case of laser compound processing, the mechanism of machining the hole is more complicated. Future research is needed to explain this phenomenon. The EDS graph in Fig. 7 b shows that the contents of the main elements on the inside surface of the hole are consistent with the matrix elements, which further confirms that there is no recast layer or HAZ in the hole.

## 4 Conclusion

In this paper, a novel method of laser machining combined with high temperature chemical etching is presented. In this method, laser processing and chemical etching are combined. A mixture of 4 mol/L  $\text{NaNO}_3$  and 3 mol/L HCl was chosen because it minimally reacts with the matrix at room temperature but reacts rapidly at high temperatures. The comparison under the three processing conditions shows that the hole can be processed more efficiently, and the defect layer can be removed more easily in the chemical solution. To drill holes with a smaller taper, the defocusing distance should be 0  $\mu\text{m}$  in the drilling stage and  $-60\ \mu\text{m}$  in the high temperature chemical stage. From what has been discussed above, a hole without a recast layer or an HAZ can be obtained. However, a honeycomb structure was present due to the non-directionality and complication of the laser combined chemical reactions.

**Funding information** This work was supported by the National Natural Science Foundation of China [No. 51775289]; the Major Basic Research Program of the Natural Science Foundation of Shandong, China [No. ZR2018ZB0524]; the Special Fund for Taishan Scholars Project [No. ts201511038]; the National Science and Technology Major Project of the Ministry of Science and Technology of China under Award [No. 2016ZX05065-001]; the Shandong Key R&D Program [No. GG201809140095]; the Applied Basic Research Program of Qingdao [No. 17-1-1-91-jch].

## References

- Peng JQ, Zhang HT, Li YF (2015) Review of blade materials for IGT. *Procedia Eng* 130:668–675. <https://doi.org/10.1016/j.proeng.2015.12.295>
- Ahn J, Schobeiri MT, Han JC, Moon HK (2007) Effect of rotation on leading edge region film cooling of a gas turbine blade with three rows of film cooling holes. *Int J Heat Mass Transf* 50:15–25. <https://doi.org/10.1016/j.ijheatmasstransfer.2006.06.028>
- Biermann D, Bücken M, Tiffe M, Özkaya E (2017) Experimental investigations for a simulative optimization of the cutting edge design of twist drills used in the machining of Inconel 718. *Procedia Manuf.* 14:8–16
- Bellotti M, Qian J, Reynaerts D (2018) Enhancement of the micro-EDM process for drilling through-holes. *Procedia CIRP* 68:610–615. <https://doi.org/10.1016/j.procir.2017.12.123>
- Chien WT, Hou SC (2007) Investigating the recast layer formed during the laser trepan drilling of Inconel 718 using the Taguchi method. *Int J Adv Manuf Technol* 33:308–316. <https://doi.org/10.1007/s00170-006-0454-1>
- Niu S, Qu N, Fu S, Fang X, Li H (2017) Investigation of inner-jet electrochemical milling of nickel-based alloy GH4169/Inconel 718. *Int J Adv Manuf Technol* 93:2123–2132. <https://doi.org/10.1007/s00170-017-0680-8>
- Stimpson CK, Snyder JC, Thole KA, Mongillo D (2017) Effectiveness measurements of additively manufactured film cooling holes. *J Turbomach* 140:011009. <https://doi.org/10.1115/1.4038182>
- Imran M, Mativenga PT, Gholinia A, Withers PJ (2015) Assessment of surface integrity of Ni superalloy after electrical-discharge, laser and mechanical micro-drilling processes. *Int J Adv Manuf Technol* 79:1303–1311. <https://doi.org/10.1007/s00170-015-6909-5>
- Romoli L, Vallini R (2016) Experimental study on the development of a micro-drilling cycle using ultrashort laser pulses. *Opt Lasers Eng* 78:121–131. <https://doi.org/10.1016/j.optlaseng.2015.10.010>
- Rashed CAA, Romoli L, Tantussi F, Fuso F, Bertocini L, Fiaschi M, Allegrini M, Dini G (2014) Experimental optimization of micro-electrical discharge drilling process from the perspective of inner surface enhancement measured by shear-force microscopy. *CIRP J Manuf Sci Technol* 7:11–19. <https://doi.org/10.1016/j.cirpj.2013.10.002>
- Tagliaferri F, Genna S, Leone C, Leone C, Palumbo B, De Chiara G (2017) Experimental study of fibre laser microdrilling of aerospace superalloy by trepanning technique. *Int J Adv Manuf Technol* 93:3203–3210 <https://doi.org/10.1007/s00170-017-0773-4>
- Li W, Zhang R, Liu Y, Wang C, Wang J, Yang X, Cheng L (2016) Effect of different parameters on machining of SiC/SiC composites via pico-second laser. *Appl Surf Sci* 364:378–387. <https://doi.org/10.1016/j.apsusc.2015.12.089>
- Genna S, Tagliaferri F, Leone C, Palumbo B, De Chiara G (2017) Experimental study on fiber laser microcutting of Nimonic 263 superalloy. *Procedia CIRP* 62:281–286. <https://doi.org/10.1016/j.procir.2016.06.109>
- Zhang Y, Shen Z, Ni X (2014) Modeling and simulation on long pulse laser drilling processing. *Int J Heat Mass Transf* 73:429–437. <https://doi.org/10.1016/j.ijheatmasstransfer.2014.02.037>
- Matti RS, Kaplan AFH (2015) Post-modelling of images from a laser-induced wavy boiling front. *Appl Surf Sci* 357:2277–2284. <https://doi.org/10.1016/j.apsusc.2015.09.226>
- Matti RS, Kaplan AFH (2014) Analysis of moving surface structures at a laser-induced boiling front. *Appl Surf Sci* 317:560–567. <https://doi.org/10.1016/j.apsusc.2014.08.190>
- Wang J, Sun SF, Liu QY, Shao J, Zhang FY, Zhang Q (2019) Effects of laser processing parameters on glass light guide plate scattering

- dot performance. *Opt Laser Technol* 115:90–96. <https://doi.org/10.1016/j.optlastec.2019.01.033>
18. Kruusing A (2004) Underwater and water-assisted laser processing: part 1 - general features, steam cleaning and shock processing. *Opt Lasers Eng* 41:307–327. [https://doi.org/10.1016/S0143-8166\(02\)00142-2](https://doi.org/10.1016/S0143-8166(02)00142-2)
  19. Gurevich EL, Hoppius JS, Maragkaki S, Gregorcic P, Kanitz A (2018) Optimization of femtosecond laser processing in liquids. *Appl Surf Sci* 467–468:255–260. <https://doi.org/10.1016/j.apsusc.2018.10.121>
  20. Letzel A, Santoro M, Frohleiks J, Ziefuss AR, Stefan R, Plech A, Fazio E, Neri F, Barcikowski S, Gokce B (2019) How the re-irradiation of a single ablation spot affects cavitation bubble dynamics and nanoparticles properties in laser ablation in liquids. *Appl Surf Sci* 473:828–837. <https://doi.org/10.1016/j.apsusc.2018.12.025>
  21. Bao J, Long Y, Tong Y, Yang X, Zhang B, Zhou Z (2016) Experiment and simulation study of laser dicing silicon with water-jet. *Appl Surf Sci* 387:491–496. <https://doi.org/10.1016/j.apsusc.2016.06.135>
  22. Ye Y, Wu M, Ren X, Zhou J, Li L (2018) Applied surface science hole-like surface morphologies on the stainless steel surface through laser surface texturing underwater. *Appl Surf Sci* 462:847–855. <https://doi.org/10.1016/j.apsusc.2018.08.117>
  23. Liu Y, Wei R, Ding W, Wang X, Song W, Sheng Z, Dai J, Liang C, Zhu X, Sun Y (2019) Porous Fe<sub>3</sub>O<sub>4</sub> thin films by pulsed laser assisted chemical solution deposition at room temperature. *Appl Surf Sci* 478:408–411. <https://doi.org/10.1016/j.apsusc.2019.01.282>
  24. Lv J, Dong X, Wang K, Duan W, Fan Z, Mei X (2016) Study on process and mechanism of laser drilling in water and air. *Int J Adv Manuf Technol* 86:1443–1451. <https://doi.org/10.1007/s00170-015-8279-4>
  25. Li L, Achara C (2004) Chemical assisted laser machining for the minimisation of recast and heat affected zone. *CIRP Ann - Manuf Technol* 53:175–178. [https://doi.org/10.1016/S0007-8506\(07\)60672-6](https://doi.org/10.1016/S0007-8506(07)60672-6)
  26. Li X, Zhou J, Wang K (2018) Research on removal characteristics of recast layer of laser-electrolytic machining on small holes. *Int J Adv Manuf Technol* 97:3903–3914. <https://doi.org/10.1007/s00170-018-2014-x>
  27. Stephen A (2011) Mechanisms and applications of laser chemical machining. *Phys Procedia* 12:261–267. <https://doi.org/10.1016/j.phpro.2011.03.132>
  28. Zhang Y, Xu Z, Zhu D, Qu N, Zhu Y (2016) Drilling of film cooling holes by a EDM/ECM in situ combined process using internal and side flushing of tubular electrode. *Int J Adv Manuf Technol* 83:505–517. <https://doi.org/10.1007/s00170-015-7575-3>
  29. Khuat V, Ma Y, Si J, Chen T, Chen F, Hou X (2014) Fabrication of through holes in silicon carbide using femtosecond laser irradiation and acid etching. *Appl Surf Sci* 289:529–532. <https://doi.org/10.1016/j.apsusc.2013.11.030>

**Publisher's note** Springer Nature remains neutral with regard to jurisdictional claims in published maps and institutional affiliations.